Technical Communication

Estimate Pulsed Laser Drilling Aluminum Nitride (AlN) Ceramic: A Thermal Simulation and Experimental Analyze

Ming-Fei Chen[1], Jun-Han Lin[1], and Wen-Tse Hsiao[*2]

[1]*Department of Mechatronics Engineering, National Changhua University of Education, Taiwan, No.1, Jin-De Road, Changhua City, 50007, Taiwan*
[2]*Taiwan Instrument Research Institute, National Applied Research Laboratories, Taiwan, No.20, R&D Rd. VI, Hsinchu Science Park, Hsinchu, 30076, Taiwan*
[*]*Corresponding author's e-mail: wentse@narlabs.org.tw*

This study performed thermal effect analysis and an experimental verification of the effects of ultrafast picosecond pulsed laser micro-drilling of aluminum nitride ceramic substrates. COMSOL Multiphysics was used to determine a laser drilling thermal field distribution; develop a thermal conductivity model; and further analyze the effects of different laser power levels, pulse durations, and focal points on hole diameter and hole depth after drilling. After results were obtained from the theoretical model, verification was performed through experiments. Using single-variable changes in laser power, laser pulse duration, and focal point, this study determined the relationships between each parameter and the machining effect and compared the simulation and experimental results.
DOI: 10.2961/jlmn.2022.02.3001
Keywords: thermal effect analysis, ultrafast picosecond pulsed laser, micro-drilling, aluminum nitride (AlN) ceramic, COMSOL Multiphysics

1. Introduction

With changes in consumption habits, the demand for consumer electronics such as smartphones, liquid crystal displays, laptop and tablet computers, digital cameras, handheld game consoles, and lighting devices has increased. Passive components play key roles in consumer electronics by enabling multifunctionality; smartphones, for instance, require at least 750 passive components. Because aluminum nitride (AlN) and aluminum oxide ceramic substrates have favorable mechanical, physical, electronic, and thermal conductivity properties, they are often used as base materials for passive components.

During the treatment of brittle materials, diamond grinding wheels are often used for grinding and shaping substrates. These processes can easily cause microcracks in the substrate and induce fragments to stick to the surface of the processed material. Furthermore, contact machining (involving the use of cutting tools and materials) easily results in the wearing of cutting tools and residual stress in substrates, thus affecting product efficacy. Nontraditional machining processes (e.g., wet chemical etching, electrochemical machining, electrical discharge machining, water-assisted machining, and laser processing) have been used in removal machining processes for brittle material. Some literatures were described laser processing of hard and brittle materials. Stavropoulos et al. [1] proposed femtosecond laser pulse material processing method for understanding ablation physical processes by using molecular dynamics-based approach. Choo et al. [2] used short-pulse KrF laser drilling of silicon workpiece both in air and under water. The experimental results indicated that the ablation depth was increased with the laser fluence increasing, the variation being nonlinear. Moreover, the ablation depth was dependent on the number of pulses, increasing with increasing number of pulses. Zheng et al. [3] established the thermo-mechanical coupled model to obtain temperature history, phase transformation stress and thermal stress during laser drilling process. To discuss the laser beam scanning, laser intensity attenuation, the nonlinear relationship between depth and time of drilling. Zhang et al. [4] proposed the precision control the taper of microholes under percussion laser drilling by molecular dynamics simulation. This method can analyze the cluster behaviour during femtosecond laser ablation and the results provide guidance for the optimization of the femtosecond laser percussion drilling technology. Yang et al. [5] evaluated electron and lattice temperature based on the traditional two-temperature model for understanding the interaction between the femtosecond laser and the Ni-based and Fe-based superalloys laser processing parameter optimization. Winter et al. [6] reported the time-resolved (from femtoseconds to microseconds) surface dynamics analytical techniques on aluminum and stainless steel. Ren et al. [7] used a water-assisted femtosecond laser drilling method to drill holes in alumina ceramics. The morphology, diameter, taper angle, cross-section area, and sidewall characteristics of the holes were investigated, and the hole characteristics obtained in the presence of air were compared with those obtained under water assistance. The results indicated that the drilling efficiency and quality of the holes improved significantly by using the water-assisted femtosecond laser drilling method, and the effect was considerably obvious at lower pulse repetition rates. Li et al. [8] fabricated and drilled micro-scale structures on K24 superalloy using femtosecond laser, due to its femtosecond laser excellent performance of the ultrashort pulse width and ultrahigh

peak power. The experimental results indicated that the low fluences (1-10 J/cm^2), laser-induced periodical surface structures (LIPSSs) occur at the region of laser irradiation. In the high fluences (121-605 J/cm^2), the holes with high aspect ratio larger than 10:1. Cheng et al. [9] investigated one-dimensional two-temperature model with temperature-dependent material properties for a copper foil surface by a single femtosecond laser pulse of duration of 120 fs and wavelength of 800 nm. Based on the theoretically and experimentally, the results indicated that the simulation ablation depth agree with experimental measurements, the fluence were ranging from 6.1 to 63.4 J/cm^2. Zhu et al. [10] proposed the material removal process during picosecond laser micro-grooving of single crystalline germanium were explored by developing a 2D two-temperature model. Cheng et al. [11] presented the experimental observations, mathematical models, and the behind physics for ultrafast laser materials micromachining. The effect parameters in the ultrafast laser micromachining including laser pulse duration, plasma, and polarization. Zhao et al. [12] created a heat conduction model for nanosecond laser processing of Al_2O_3 by COMSOL multi-physics. The real temperature distributions were experimentally verified using an infrared thermometer. Zhang et al. [13] proposed the machine learning model for femtosecond laser trepan drilling processes for enhancing the geometric quality (taper), recast layer, and processing efficiency of micro-holes. Alavi and Harimkar [14] used ultrasonic vibration–assisted laser drilling for stainless steel surface processing to remove the plasma melt produced through heat. Their experimental results indicated that when the ultrasonic output frequency was increased, the laser apertures were smaller and the drilling depth was increased. Meng et al. [15] used a 20-W fiber laser to perform micro hole array processing on titanium alloy substrates to increase the adhesion of biomaterials on substrates. Their analysis results indicated that optimal adhesion performance was achieved at a focal point of 0 mm, an average power of 16 W, and a laser operation time of 1 ms. Finally, they soaked a test piece in electrified hydroxyapatite to determine the deposition results. Romoli and Vallinib [16] conducted an optimization study using an ultrashort pulsed laser to drill stainless steel; the drilling process was divided into test drilling, hole diameter expansion, and precision finish stages. Their findings revealed that angled cutting methods, compared with regular turning, could more efficiently remove material. The produced hole conicity was then minimized with finishing. The final drilling method could, within 3.75 s, drill a cylindrical hole with a diameter of 180 μm into a 350-μm-thick stainless-steel sheet without leaving any burrs in the inner wall. Said-Bacar et al. [17] used COMSOL Multiphysics software to model changes in a thin silicon film on a glass substrate when heated using a laser. They first applied one-dimensional modeling to determine the film's melting, crystallization, and ablation temperatures. Subsequently, they varied the initial temperature and scanning speed to test the effects of the experimental parameters on the results. They discovered that higher ambient temperatures led to decreases in the energy density required for laser processing but that higher scanning speeds necessitated the use of a higher energy density to reach the necessary temperatures. Therefore, a suitable reduction of scanning speed strengthened the processing effects. Begic-Hajdarevic and Bijelonja [18] used a laser to conduct a drilling experiment on a tungsten alloy and performed a numerical simulation of the temperature field of the heat-affected zone. They used the finite volume method to predict the temperature distribution and heat-affected zone during laser processing. Bharatish et al. [19] used COMSOL Multiphysics and Raman spectroscopy to observe and verify the residual thermal stress caused by lasers in aluminum oxide ceramic drilling. The properties and degree of residual stress influence could be observed through the degree of damage in the heat-affected zone. They also analyzed the stretching and damage inside the hole due to residual thermal stress, thus enabling the prevention of wall cracks in the inner hole. Zhang et al. [20] used a two-dimensional (2D) model of the level-set method to simulate the laser drilling of an aluminum alloy. Considering mass loss during evaporation and boiling, they used equivalent specific heat and gas dynamics and phase change methods to execute the modeling process. The model was used to investigate the laser energy density, pulse width, drilling speed, and hole diameter and shape. They compared the experimental and simulation results. Their simulation and experimental results revealed that an increase in laser power engendered an increase in melt ejection velocity; pulse duration was the primary factor affecting the hole walls. Chen et al. [21,22] used ANSYS to establish a temperature field model of the laser drilling of a ceramic substrate and isolate a multilayer stack of copper–indium—gallium–selenide (CIGS)-based thin-film solar cells. They used ANSYS APDL to establish a mesh model for the simulation of the thermal distribution of the lasers acting on the material. Their results indicated that when the number of pulses reached 9 or 10, the ceramic substrate was completely perforated. For the multilayer stack of the CIGS-based thin-film solar cells, the simulation and experimental results indicated that the laser processing temperature was between 2896 ℃ and 2248 ℃. Dal and Fabbro [23] used COMSOL to simulate laser welding separately through heat transfer modeling and multiphysics modeling. They concluded that the parameters were more complex in simulations that more closely reflected reality. Optimal simulations must consider not only the multiple reflections of lasers, heat transfer, gas–liquid flow, and free-boundary displacements but also the interaction between electromagnetic waves and the material, which results in a disproportionately long simulation time. Additionally, the simulation results emphasized only the material temperature and hole diameter and shape.

This study used Nd:YAG lasers to remove material from the surface of AlN ceramic substrates; material removal was achieved through the interactions between the laser beams and the AlN ceramic substrates, resulting in the high-temperature melting of the materials and their removal from the ceramic surface. The study used finite element analysis to determine the surface loading of a Gaussian heat source and to examine the temperature distribution during the laser drilling of the AlN ceramic sheet in order to obtain the optimal laser processing parameters and heat source arrangement, which can be used to enhance the efficiency of the process.

2. Finite element analysis of heat transfer theory

Heat conduction theory was used to analyze the internal energy exchange caused by the temperature gradient created during laser drilling. Fourier's law was used for estimation, as presented in Eq. (1):

$$q^{*\prime} = -k\frac{dT}{dx} \tag{1}$$

where q^* is the heat flow density (W/m^2), k is the thermal conductivity of the material (W/m-℃), and $\frac{dT}{dx}$ is the temperature gradient in that direction.

Using the relationship between material and laser processing parameters (such as laser power density, spot size, pulse duration, and the thermal parameter of the material), this study established a mathematical model to predict the temperature field distribution during processing in order to obtain the temperature trend for laser processing. The Gaussian energy density distribution produced by a laser pulse can be derived as shown in Eq. (2), where r indicates the laser beam radius, which is defined in Eq. (3) [11,12]:

$$I(x,y,z,t) = \frac{2\alpha P_P}{\pi r^2}\exp\left[-\frac{2(x^2+y^2)}{r^2}\right]\delta(t) \tag{2}$$

$$r = \frac{d}{2}\left[1+(M^2\frac{4\lambda(Z_m+f_c)}{\pi d^2})\right] \tag{3}$$

where α is the absorption coefficient of the material, P_P is the instantaneous power of the laser, $\delta(t)$ is the impulse function, d is the beam diameter, f_c is the focal distance of the focal lens, Z_m is the melt depth, and λ is the wavelength of the laser light.

The initial temperature of a simulation material can be defined as indicated in Eq. (4):

$$t = 0, T(t) = T_0 \tag{4}$$

where T_0 denotes the room temperature, which was set to 27ºC during the drilling of the AlN ceramic substrates (i.e., at laser time t = 0, it can be regarded as the ambient temperature).

3. Experimental laser drilling system, AlN ceramic substrate modeling, and thermal analysis conditions of laser drilling using COMSOL

A pulsed picosecond laser system was used for AlN plate drilling. Table 1 presents a summary of the specifications of the experimental system.

This study used a two-dimensional mesh model (length: 0.6 mm; width: 0.5 mm). COMSOL Multiphysics was employed to perform a temperature field analysis of the laser drilling process based on transient heat transfer and a time-dependent model. The AlN ceramic substrates had a thickness of 380 μm and were fabricated by LEATEC Fine Ceramics Co., Ltd., Taiwan. Table 2 presents the physical properties of the AlN ceramic substrates. Fig. 1 illustrates the finite element analysis process for laser drilling.

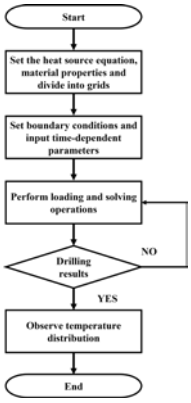

Fig. 1 Simulation flowchart of the finite element analysis process.

Table 1 Specification of pulsed picosecond laser system.

Item	Values
Wavelength (nm)	1064
Pulse repetition rate (kHz)	400 ~ 1000
Pulse width (ps)	< 15 ps
Spatial Mode	TEM_{00} (M^2<1.4)
Polarization ratio	>> 100:1
Output beam diameter (μm)	~ 3000
Focal position beam diameter (μm)	~ 140

First, the laser heat source and conduction method were defined, and the material absorption rate, heat conduction coefficient, specific heat, and materials density were set. After the establishment of a mesh model, the laser drilling time was changed and loading calculations were performed. The boundary conditions assumed for the finite element analysis were as follows:

a) The material was homogeneous and possessed isotropic heat transfer properties.
b) The laser-pulse-affected zone was axisymmetric. Because the depth of laser drilling extended downward along the *z*-axis, the model used 2D symmetry to simulate the laser drilling process.
c) The laser energy distribution was based on the TEM_{00} Gaussian energy distribution.
d) The plasma effect produced by the laser action was ignored.
e) Vaporized material would not interfere with the input laser beam.
f) The reflections produced by the laser illumination were negligible.

Table 2 Physical properties of the AlN ceramic substrate.

Item	Parameters
Density (g/cm^3)	3.2
Thermal conductivity (W/mK)	30
Thermal expansion (10^{-6}/ ºC)	4.4
Specific heat capacity (J/kg* ºK)	730
Melt point (ºC)	2400

Because substrate absorptivity affects thermal analysis results, the reflectance spectra of the A1N substrates were measured using a Jasco V670 spectrophotometer (Jasco

Inc., MD, USA) prior to the experiment. The derived spectral curve indicated that during the laser drilling of the substrates, the reflectance levels observed under a 1064-nm wavelength light source was approximately 41%. Through Eq. (5), this study determined that the absorption rates of the substrates was approximately 59%:

$$A=1-R-T \quad (5)$$

4. Thermal field simulation and experimental verification of the effect of laser power on AlN ceramic substrate drilling

In the simulation, the pulse duration and focal point were maintained constant, and the laser power was adjusted to analyze its effect on the drilling of the AlN substrates. Table 3 presents the related parameter settings.

Table 3 Effect on the laser power for drilling AlN ceramic substrate.

Item	Parameters
Laser power (Watt)	5, 10, 15, 20, 25, 30, 35
Focal point	at top surface
Pulse duration (μs)	10000

The laser power was adjusted from 5 to 35 W. Figs. 2 and 3 illustrate the COMSOL simulation results. According to the thermal field distributions in Fig. 2, increasing the power resulted in an increased hole diameter and the expansion of the heat-affected zone. When the laser power was 25 W, the AlN substrate could be penetrated. Figs. 4 and 5 display the features and cross sections of the access and exit holes drilled using different laser power levels. When the laser power was increased, the depth and diameter of the hole increased; this was consistent with the simulation. Fig. 6 displays a plot of the diameters of the top and bottom holes observed when different laser power levels were employed. Penetration was possible when the laser power was 25 W.

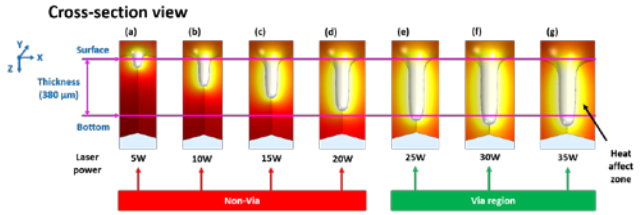

Fig. 2 Thermal field distribution under different laser powers using COMSOL Multiphysics software. (a) 5 W, (b) 10 W, (c) 15 W, (d) 20 W, (e) 25 W, (f) 30 W, (g) 35 W.

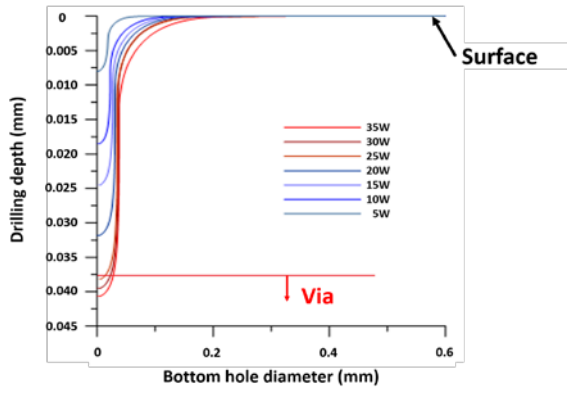

Fig. 3 Drilling depth curves for AlN ceramic substrate under different laser powers.

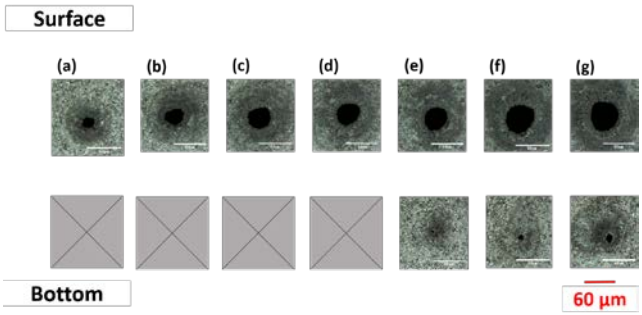

Fig. 4 Optical microscope images of top and bottom holes in AlN ceramic substrate under different laser powers. (a) 5 W, (b) 10 W, (c) 15 W, (d) 20 W, (e) 25 W, (f) 30 W, (g) 35 W.

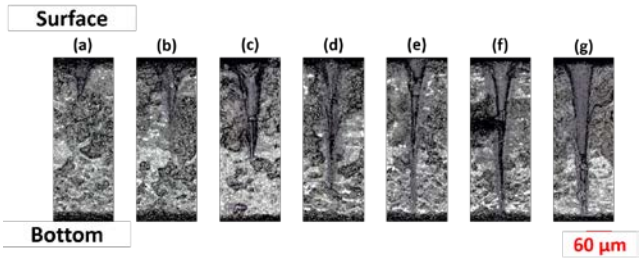

Fig. 5 Cross-section of AlN ceramic substrate under different laser powers: (a) 5 W, (b) 10 W, (c) 15 W, (d) 20 W, (e) 25 W, (f) 30 W, and (g) 35 W.

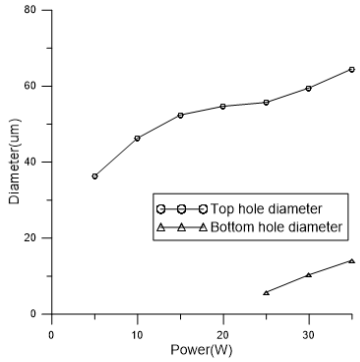

Fig. 6 Top and bottom hole dimeters in AlN ceramic substrate under different laser powers.

In the simulation, the laser power and focal point were maintained constant, and the laser pulse duration was adjusted to analyze its effect on the AlN substrate drilling process. Table 4 presents the related parameter settings.

Table 4 Effect on the pulse duration for drilling AlN ceramic substrate.

Item	Parameters
Laser power (Watt)	25
Focal point	at top surface
Pulse duration (μs)	1000, 2000, 3000, 4000, 5000, 6000, 7000, 8000, 9000, 10000, 15000, 20000, 25000

During the simulation and experiment, the laser power was 25 W, and the focal point was the AlN ceramic substrate surface. Figs. 7 and 8 display the cross-sectional thermal field distributions and drilling depths obtained us-

ing COMSOL. As demonstrated by the simulation results, when the pulse duration was increased, the drilling depth also increased; penetration was observed at a duration of 5000 μs. Figs. 9 and 10 show the single-variable experimental results and the effect of pulse duration on hole diameter. The experimental results revealed that penetration was nearly impossible at pulse durations shorter than 5000 μs and that the hole diameters did not change substantially when the pulse duration exceeded 5000 μs. Only the diameter of the bottom hole increased slightly as the pulse duration increased. After the pulse duration reached 15000 μs, no changes in diameter were observed.

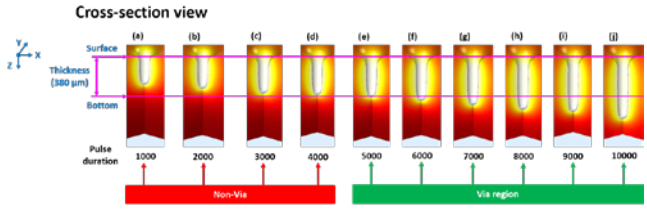

Fig. 7 Thermal field distribution under different laser pulse durations using COMSOL (a) 1000 μs, (b) 2000 μs, (c) 3000 μs, (d) 4000 μs, (e) 5000 μs, (f) 6000 μs, (g) 7000 μs, (h) 8000 μs, (i) 9000 μs, and (j) 10000 μs.

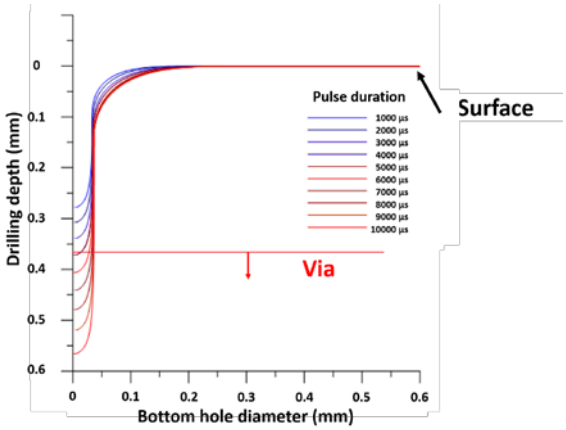

Fig. 8 Drilling depth curves for AlN ceramic substrate under different laser pulse durations.

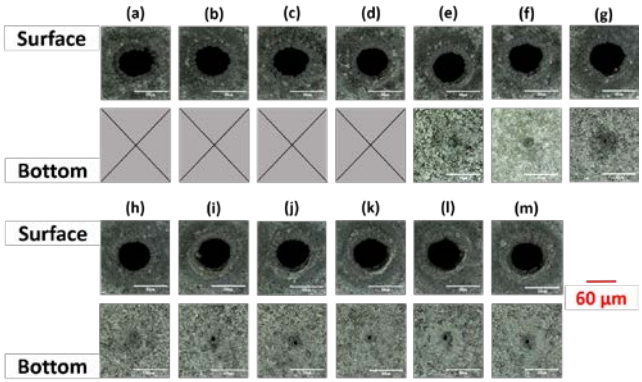

Fig. 9 Optical microscopy images of entry and exit holes in AlN ceramic substrate under different laser pulse durations: (A)1000 μs, (b) 2000 μs, (c) 3000 μs, (d) 4000 μs, (e) 5000 μs, (f) 6000 μs, (g) 7000 μs, (h) 8000 μs, (i) 9000 μs, (j) 10000 μs, (k) 15000 μs, (l) 20000 μs, and (m) 25000 μs.

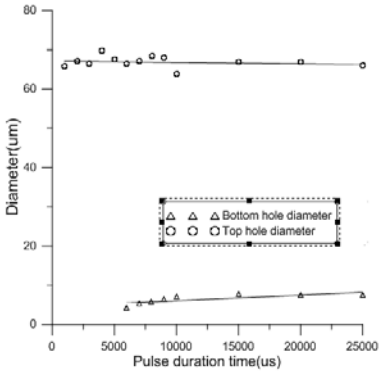

Fig. 10 Entry and exit hole diameters in AlN ceramic substrate under different laser pulse durations.

Simulations could not be performed for out-of-focus conditions; thus, the focal point was directly altered in the drilling experiments. The laser power used was 25 W, and the laser duration was 10000 μs. Table 5 lists the experimental parameters.

Table 5 Effect on the focal point for drilling AlN ceramic substrate.

Item	Parameters
Laser power (Watt)	25
Focal point (mm)	+0.75, +0.5, +0.25, 0, -0.25, -0.5, -0.75
Pulse duration (μs)	10000

(Note: + indicates out-of-focus [above substrate], − indicates out-of-focus [below substrate])

Figs. 11 and 12 display the experimental results and the influence of the laser focal point on the drilling outcome. The focal point considerably affected the top- and bottom-hole diameters. The effect was most favorable when the focal point was 0 mm (i.e., on the surface of the material). Overall, the results trended toward in focus. When the laser was both in focus and out of focus, the top hole was wider and the bottom hole was narrower.

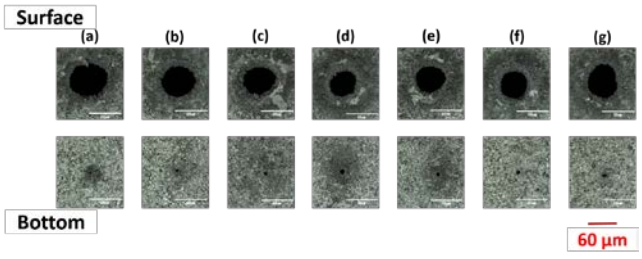

Fig. 11 Optical microscopy images of top and bottom holes in AlN ceramic substrate under different laser focal points: (a) +0.75 mm, (b) +0.5 mm, (c) +0.25 mm, (d) 0 mm, (e) -0.25 mm, (f) -0.5 mm, (g)-0.75 mm.

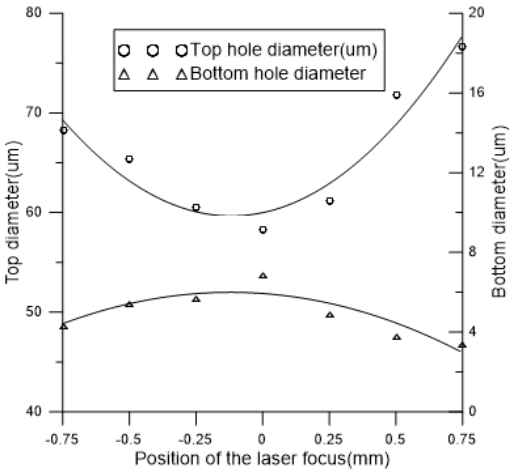

Fig. 12 Top and bottom hole diameters in AlN ceramic substrate under different laser focal points.

5. Conclusions

This study successfully used COMSOL Multiphysics to simulate the thermal field distribution during the laser drilling of AlN ceramic substrates and the corresponding changes in material properties. The output parameters of the laser source were set, and the laser was applied to the surface of the material. In general, when the processing temperature reaches the melting point of a material, the material melts downward. Phase changes were thus used to change the heating zone according to changes in the material. Consequently, the simulation results closely reflected those of the actual experiment.

According to the simulation and experimental results, the laser power had the strongest effect on the drilling process, followed by the focal point. The laser pulse duration had the weakest effect, primarily because after a melt hole is generated through laser melting of the material, the wall of the hole melts, leading to material buildup inside the hole. Consequently, a longer laser pulse could not expand the hole diameter.

Acknowledgement

The authors thank the National Science and Technology Council of Taiwan for financially supporting this research under contract nos. NSTC 103-2221-E-018-004-MY2 and NSTC 110-2622-E-492-016.

References

[1] P. Stavropoulos, K. Efthymiou, and G. Chryssolouris, Procedia CIRP, 3, (2012) 471.
[2] K.L. Choo, Y. Ogawa, G. Kanbargi, V. Otra, L.M. Raff, and R. Komanduri, Mater. Sci. Eng. A, 372, (2004) 145.
[3] C. Zheng, K. Zhao, H. Shen, X. Zhao, and Z. Yao, J. Mater. Process. Technol., 282, (2020) 116678.
[4] Z. Zhang, Z. Xu, C. Wang, S. Liu, Z. Yang, Q. Zhang, and Wei Xu, Opt. Laser Technol., 139, (2021) 106968.
[5] Z. Yang, P. Ji, Z. Zhang, Y. Ju, Z. Wang, Q. Zhang, C. Wang, and W. Xu, Opt. Commun., 475, (2020) 126237.
[6] J. Winter, S. Rapp, M. Spellauge, C. Eulenkamp, M. Schmidt, and H.P. Huber, Appl. Surf. Sci., 511, (2020) 145514.
[7] N. Ren, K. Xia, H. Yang, F. Gao, and S. Song, Ceram. Int., 47, (2021) 11465.
[8] Q. Li, L. Yang, C. Hou, O. Adeyemi, C. Chen, and Y. Wang, Opt. Lasers Eng., 114, (2019) 22.
[9] C.W. Cheng, S.Y. Wang, K.P. Chang, and J.K. Chen, Appl. Surf. Sci., 361, (2016) 41.
[10] H. Zhu, Z. Zhang, J. Xu, Y. Ren, Z. Zhu, K. Xu, Z. Wang, and C. Wang, J. Manuf. Process., 69, (2021) 351.
[11] J. Cheng, C.S. Liu, S. Shang, D. Liu, W. Perrie, G. Dearden, and K. Watkins, Opt. Laser Technol., 46, (2013) 88.
[12] W. Zhao, X. Mei, and Z. Yang, Ceram. Int., 48, (2022) 4474.
[13] Z. Zhang, S. Liu, Y. Zhang, C. Wang, S. Zhang, Z. Yang, and W. Xu, Opt. Laser Technol., 148, (2022) 107688.
[14] S.H. Alavi and S.P. Harimkar, Manuf. Lett., 4, (2015) 1.
[15] L.N. Meng, A.H. Wang, Y. Wu, X. Wang, H.B. Xia, and Y.N. Wang, J. Mater. Process. Technol., 222, (2015) 335.
[16] L. Romolia and R. Vallinib, Opt. Lasers Eng., 78, (2016) 121.
[17] Z. Said-Bacar, Y. Leroy, F. Antoni, A. Slaoui, and E. Fogarassy, Appl. Surf. Sci., 257, (2011) 5127.
[18] D. Begic-Hajdarevic and I. Bijelonja, Procedia Engineering, 100, (2015) 384.
[19] A. Bharatish, H.N.N. Murthy, G. Aditya, B. Anand, B.S. Satyanarayana, and M. Krishna, Opt. Laser Technol., 70, (2015) 76.
[20] Y. Zhang, Z. Shen, and X. Ni, Int. J. Heat Mass Transf., 73, (2014) 429.
[21] M.F. Chen, W.T. Hsiao, M.C. Wang, K.Y. Yang, and Y.F. Chen, Int. J. Adv. Manuf. Technol., 81, (2015) 1723.
[22] M.F. Chen, W.T. Hsiao, M.C. Wang, Y.F. Chen, and C.M. Lo, Opt. Quantum Electron., 49, (2017) 85.
[23] M. Dal and R. Fabbro, Opt. Laser Technol., 78, (2016) 2.
[24] S. Mishra and V. Yadava, Opt. Laser Technol., 48, (2013) 461.

(Received: February 7, 2022, Accepted: September 2, 2022)